Turkish Journal of Engineering
https://dergipark.org.tr/en/pub/tuje
e-ISSN 2587-1366

Stepwise double-sided friction stir welding: an alternative for root defect mitigation in aluminium plates with lower gauge numbers

Olatunji Oladimeji Ojo *1, **Ozioma Alaba Oboro** 2

1The Federal University of Technology Akure, Industrial and Production Engineering, Nigeria, ojooladimeji90@yahoo.com
2 The Federal University of Technology Akure, Department of Mechanical Engineering, Nigeria, oziomaboro@hotmail.com

Cite this study: Ojo, O. O., & Oboro, O. A. (2024). Stepwise double-sided friction stir welding: an alternative for root defect mitigation in aluminium plates with lower gauge numbers. Turkish Journal of Engineering, 8 (4), 611-618.

https://doi.org/10.31127/tuje.1449966

Keywords
Friction stir welding
Aluminium alloy
Microstructure
Mechanical Properties
Fracture

Research/Review Article

Received: 09.03.2024
Revised: 08.04.2024
Accepted: 13.05.2024
Published: 31.10.2024

Abstract

Penetration-induced fractional unbonded defects and flow-induced root flaws are part of the discontinuities of the conventional friction stir welded (FSW'ed) aluminium alloys with limited impact assessment/clarification in literature. The novelty of this study lies in the attempt to eliminate penetration-aided root defect via a stepwise double-sided welding process as well as identify its impact on loadbearing. As a result, the stepwise double-sided FSW welding of a thick aluminium plate (6 mm) was carried out while the microstructure, strength, and fracture modes of the ensuing welds were compared with the conventional (single-sided) friction stir welded counterparts. The stepwise double-sided FSW-welded joint demonstrated better tensile strength relative to the single-sided FSW-welded counterparts owing to its material flow consolidation (two-side deformation) and elimination of penetration-induced fractional unbonded region/root defect. The welding processes do not have a noteworthy influence on the fracture location of the welds as failure ensued via the stir zones of the respective welds. Transient breaking/brittle appearance, and ductile fracture modes were noticed in the single-sided and stepwise double-sided FSW-welded samples respectively. The stepwise double-sided FSW process is recommended as a better choice for thick workpieces relative to conventional FSW to improve the weld's loadbearing resistance.

1. Introduction

Weld discontinuities are undesirable stress concentration zones responsible for crack initiation and premature weld failure in weldments. Wang et al. [1] revealed that the existence of micro-voids in the FSW'ed AA2219-T8 alloy impeded the necking capability (ductility) and decreased the maximum strain of the weld. As a result, weld defects need to be prevented or eliminated to improve the mechanical/load-bearing properties of weld structures. The notable weld discontinuities in friction stir welded or spot-welded lightweight alloys include flow-related defects (voids/holes/tunneling, a zigzag line, kissing bond, and upward flow-induced hooking defects) [2-5], tool-induced keyholes, interface bulging/lifting [6], and root defect or penetration-induced fractional unbonded region. The flow-related defects are mostly linked to insufficient plastic flow of materials owing to the low welding-induced heat input (or inappropriate selection of process parameters), and the presence of inherent oxides hindering plastic flow during the friction stir welding (FSW) process [7]. Wang et al. [8] also reported that weld defects are caused by the inhomogeneous heat distribution and the significant disproportion between the flow-aided stresses of the shoulder- and pin-driven flows. The exit holes left by the pin tools after the friction stir welding (FSW) are referred to as keyholes, which are major stress raisers but the modifications of FSW processing as well as a change of the tool profile have been effective in eliminating keyhole defects in FSW'ed joints [9]. The less-reported category of defects in friction stir welds is the root defect, which is primarily caused by the penetration level of the pin tool, especially in thick base materials. The penetration-induced fractional unbonded region is typically left at the vortex/root (pin end) regions of FSW'ed joints. The severity of the root defect depends on the level of the fractional unbonded region but clarification on this class of weld defect has received inadequate consideration in literature. This study attempts to eliminate the penetration-induced fractional unbonded region via the use of a stepwise double-sided friction stir welding (SDFSW) and equally identify the impact of the fractional unbonded region on the loadbearing property of the FSW'ed Al alloy.

Process parameter optimization is a notable manner for eliminating flow-related defects and controlling the inherent heat input in the FSW'ed aluminium alloys. The heat input could easily cause thermal softening, phase dissolution, and over-aging of the Cu/Li ratio, which have detrimental consequences on the mechanical performances of the joint [10]. The use of auxiliary energy-assisted friction stir welding is gradually being employed to soften and improve the viscoplasticity of materials toward mitigating flow-related defects in Al alloys. For instance, the hole defect in the FSW'ed AA2519 Al alloy has been effectively eliminated via the usage of the TIG arc-assisted friction stir welding technique in the studies of Yi et al. [7]. This welding option reduced the Joint's onion ring area and improved the mechanical-properties of the FSW'ed AA2519 joint due to the higher density of fine θ′ precipitates (hardening phase) in the weld.

Double-sided FSW (DFSW) is a variant of the traditional single-sided FSW (SFSW) for improving material flow, and microstructural homogeneity towards improving weld quality [11]. The DFSW has been recognized as a joining option capable of eliminating root defects typical in conventional single-sided friction stir welds. The DFSW can effectively reduce the asymmetric material flow between two adjoining plates as highlighted in the research of Rahmatian et al. [12]. The DFSW process can be performed in two ways. The first method involves the use of two rotating tools for the simultaneous welding of the upper/top and lower/bottom parts of the materials. The co- and counter-directional rotations of the lower and upper tools are established in this case [13]. This usually involves the use of a more robust friction stir welding machine. Self-supporting or semi-stationary bobbin tool FSW processes [14-27] are typical examples of the first classification of the DFSW process that have found applications in joining/welding Al and Mg alloys in literature. The second method involves a stepwise welding manner; the welding of the upper (one) side of the workpieces is carried out just like a single-sided FSW process (SFSW). Thereafter, the other side of the workpieces is welded after the rotation of the workpieces by 180°. This second category of double-sided FSW is referred to as the stepwise double-sided FSW (SDFSW) process in this paper. With the SDFSW, the complexity of the FSW machine is eliminated while a double-sided FSW process is easily attained.

Some of the past studies on the double-sided FSW process have revealed that the strength (UTS) of the refilled friction stir spot welded AA2198 alloy was comparable to counterpart fabricated with the double-sided FSSW technique [28]. The increase in the pin length during the double-sided FSW of the AA2024-T6 Al alloy was reported to reduce the weld's elongation by up to 6.5 times [29]. Azeez and Akinlabi [30] reported that excellent bonding was established in the double-sided FSW'ed AA6082/AA7075(-T6) joint. Strong tool-assisted material flow and mixing are established around the welding interface in the double-sided FSW'ed AZ31/ZK60 joint [31]. Defect-free double-sided FSW'ed AZ31B Mg alloy was obtained after the first and second passes in the studies of Thakur et al. [32]. It was acknowledged that both sides of the weld had a high degree of grain refinement. Strain hardening, better material mixing, and improved joint quality were obtained by Darmadi et al. [33]. Improved material flow due to the staggered layer structure was achieved with the use of double-sided FSW [34] while the better texture (randomized) was established due to the complicated material flow in the studies of Chen et al. [35]. Improved welding interface structure and strong mechanical interlocks were obtained via the DSFSW/processing of the AZ31/ZK60 Mg alloys [36, 37], low carbon steel [38], AA6082 [39], AA7085-T452 [40], C-Mn-Si martensitic steel [41], dissimilar Fe/Al alloys [42] and SiC/AA2014 composite [43] respectively.

Based on cost reduction/lesser machine complexity and the existing literature, the impact of the stepwise double-sided FSW (SDFSW) process on the penetration-induced fractional unbonded region (root defect) mitigation in relation to the single-sided FSW (SFSW) process still requires clarification. As a result, this paper compares the weld performances of the SDFSW and SFSW processes.

2. Method

Aluminium base plates (6 mm thick) were the materials utilized for this study. As determined by the X-ray fluorescence analysis, the composition of the base plate consists of 7.55wt% Mg, 0.01wt% Cr, 0.04wt% Mn, 0.05wt% Ni, 0.11wt% Zn, 0.022wt% Sn, 0.05wt% Sb, and Al (as the balance) while its mechanical properties are 89.8 MPa and 3.2 % (elongation). The as-received Al sheets were cleaned and machined into the 100 x 50 x 6 mm by employing a hydraulic powered guillotine. Two cut/sheared samples were brought together to form a butt configuration for the FSW welding process as illustrated in Figure 1. Two categories of FSW welding processes were employed for joining the plates. They are the SFSW and the SDFSW processes. The single-sided friction stir welding (SFSW) of the plates was carried out with a 20 mm diameter cylindrical H13 tool (with a probe height and diameter of 4.6 and 7 mm respectively). Due to the absence of the through-thickness penetration of the tool in the SFSW welds, a fractional unbonded margin is left at the reverse side/part of the weld line (in the SFSW welds). To eliminate this, the opposite side of the welded SFSW sample was subsequently turned over, clamped, and welded with a probe-less H13 tool having a diameter of 20 mm. This second welding category is denoted as stepwise double-sided FSW (SDFSW) in this research-paper as it involves the welding of both sides of the clamped plates in a stepwise manner. The diagrammatical representations of the SFSW and SDFSW processes are shown in Figure 2. Also, the pictorial images of the welding tools used for the SFSW and SDFSW processes are provided in Figure 3. The tool speeds (710 up to 1120 rpm) and travel speeds (25 up to 63 mm/min) were varied for the welding processes while the plunge depth and the tilt angle (0°) of the tool were kept unchanged.

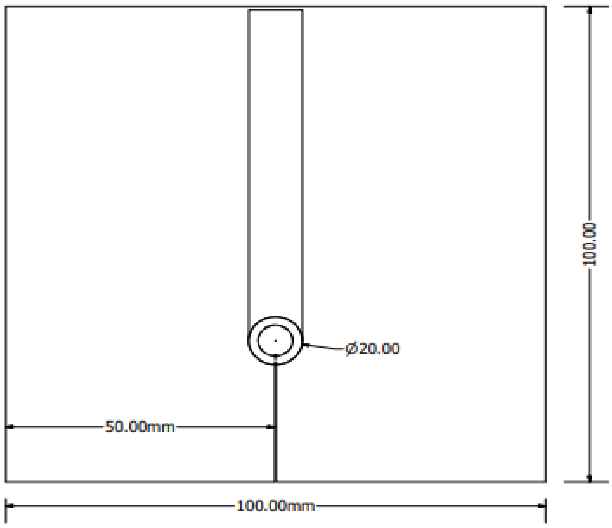

Figure 1. Schematic of the plan/butt configuration for the FSW welding process (with dimensions).

Figure 2. The H13 tool steel used for welding (a) probe tool (b) probe-less tool.

The cross-sections of the SFSW'ed and SDFSW'ed joints were prepared, ground with different emery paper grits, polished, and etched in Keller's reagent. With an optical microscope, the microstructure of the both categories of the joints were examined. The tensile test samples were machined in a manner perpendicular to the weld path (see Figure 4). The tensile tests of the SFSW'ed and SDFSW'ed joints were conducted in line with the ASTM-E8 using an INSTRON universal tensile test machine at a displacement rate of 5 mm/min under room temperature. The fractography of the tensile samples after the test was carried out with the assistance of the JOEL-JSM 7600F scanning electron microscope (SEM). This was performed for both the SFSW and SDFSW tensile samples to comprehend the weld's fracture mode.

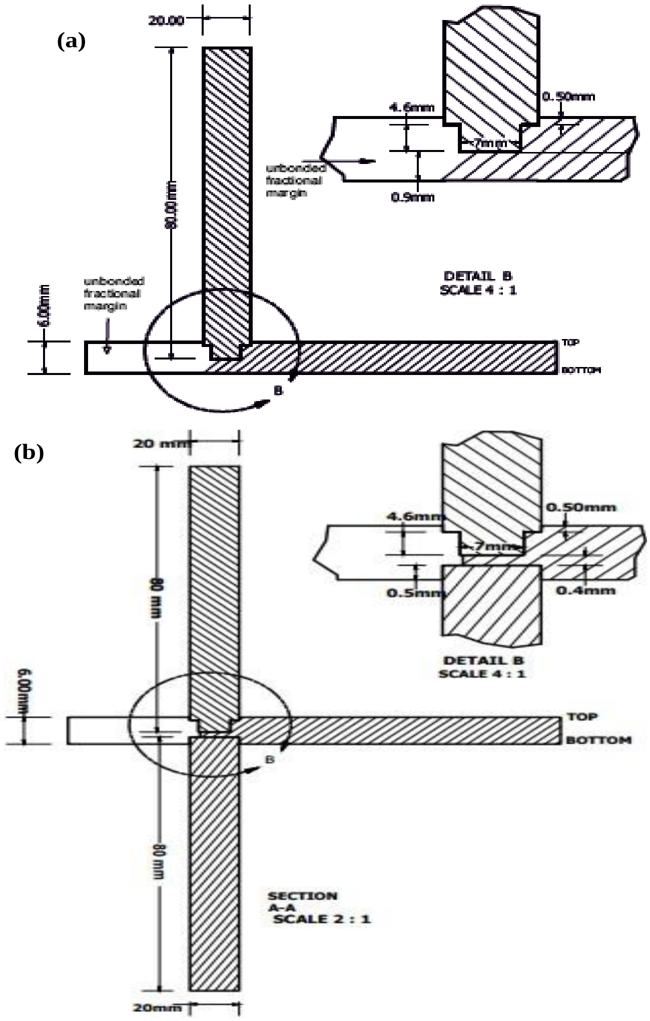

Figure 3. Diagrammatic depiction of the welding processes (a) SFSW and (b) SDFSW processes.

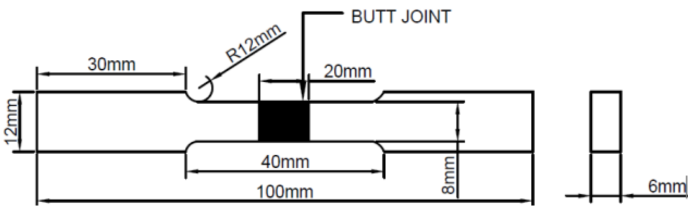

Figure 4. Schematic of the tensile specimen.

3. Results and discussion

3.1 Weld structure

Figure 5 displays the unetched macrostructures of the single-sided SFSW'ed and SDFSW'ed Al joints. Root and flow defects are present in the SFSW'ed joints in Figure 5a and 5b as a result of the thick workpiece irrespective of the process parameter's level utilized for the welding process. The region above the root-defected region shows uniformity and absence of any flow-related defect as the rotation of the tool shoulder facilitated sufficient heat/thermal input, material flow, and microstructural homogeneity in Figure 5a and 5b. Insufficient intermaterial mixing and bonding occurred at the vortex region (pin tip) of the welds and this could be associated with the gauge of the workpiece against the pin height (or penetration depth into the workpiece). The appearance of the root defects differs in the single-sided joints owing to the difference in the level of the parameters employed for the welding. However, the presence of root defects is fully eliminated in the SDFSW'ed joints in Figure 5c and 5d. This is perceptibly because of the impact of plastic deformation-induced material flow at the bottom/lower part (root-defected region) of the weld during the second phase of the joining process. Apart from the macrostructure of the welds, the assessment of the weld's microstructure is carried out.

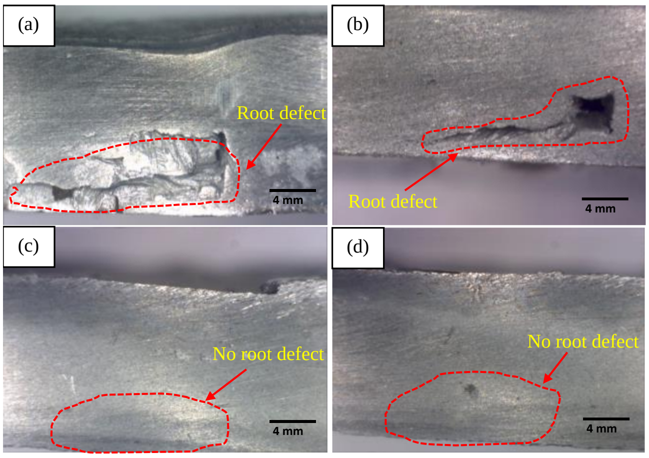

Figure 5. Macrostructure of (a) and (b) single-sided welds; (c) and (d) double-sided welds.

The microstructures of the base material as well as the friction stir welded joints at dissimilar parameter levels are provided in Figure 6. The microstructure of the base material (BM) in Figure 6a and b appears to be coarser relative to the other processed samples in Figure 6b-h. This is obviously as a result of the tool-assisted severe plastic-deformation and dynamic-crystallization effects at the stirred zones (SZ) of the welds regardless of the type of the welding process (single or double-sided weld). However, the disparity in the process parameters slightly influences the outlook of the microstructure of the welds. The changes in welding parameters have been acknowledged to affect heat generation, material flow, and the resultant microstructure of friction stir (spot) welds [44, 45]. Similarly, it has also been reported in the literature that the upsurge in the tool's rotating speed has a linear/direct impact on heat generation [46, 47]. As a result, more frictional and deformational heat input is generated by a rise in the rotating speed of the tool and this outcome aids material softening and flowability during the SFSW and the SDFSW processes. The flow behaviour of the welds is expected to be enhanced by the upsurge in the rotating speed of the tool. However, the flow pattern is not discernible at the stirred zones of the SFSW and SDFSW welds in Figure 6c-h as a result of the formation of dynamic recrystallization-induced fine (equiaxed) grains at the SZs. The second stage of the SDFSW process is envisaged to have provided consolidated flow at the second side of the weld sample. A clear distinction could not be found between the SZs of the SFSW and SDFSW processed samples in terms of visual (grain) appearance. However, the structures of the weld sample fabricated at 710 rpm/40 mm/min (both the SFSW and SDFSW welds) have no visible flow-defected zone while flow-defected zones are significant in the SFSW-processed samples (see Figure 6f and h). The flow consolidation impact of the DFSW process significantly reduced the flow defect in the sample processed at 900 and 1120 rpm. As a result, it can be concluded that the SDFSW process performs two functions, namely, flow consolidation and elimination of fractional unbonded margin.

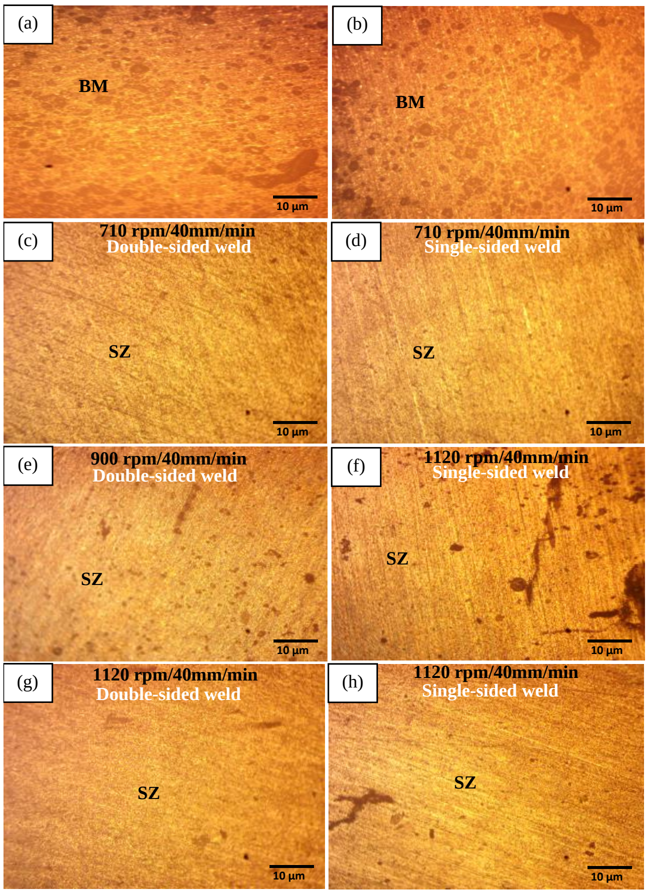

Figure 6. Microstructure of the base plate and stirred zones at different process parameters.

3.2 Tensile Results

Figure 7 reveals the plot of the tensile strength against the ratio of the tool's rotating speed (ω) to the traverse/travel speed (ν) of the SFSW and SDFSW'ed joints. The change in the ω/ν brings about a change in the strength of the welded joints irrespective of the welding categories (SFSW and SDFSW) owing to the different parameter-induced material flow behaviour and microstructural modification. The SDFSW'ed samples generally had higher tensile strength values compared to the SFSW'ed samples at 710 and 900 rpm respectively (regardless of the traverse speed) thanks to the consolidated material flow (two-sided deformation), and elimination of the penetration-induced fractional unbonded region (root defect) in the SDFSW'ed samples. At the highest rotational speed (1120 rpm) with 40 and 60 min/min travel speeds, the SDFSW process had a detrimental effect on the strength of the joint compared to the SFSW'ed counterparts. This could be attributable to the extreme heat generation at both sides of the welds.

Desirable or highest tensile strengths were obtained at the least level of the tool rotational speed (710 rpm) as compared to the other levels (900 and 1120 rpm) in both weld categories (SFSW and SDFSW processes). At 710 rpm/40 mm/min, the highest strength of 48.41 MPa was gotten in the sample fabricated with the SDFSW process while its respective SFSW'ed counterpart had a tensile strength of 34.24 MPa. This implies that the upsurge in the speed beyond 710 rpm leads to the generation of undesirable heat generation while traverse speed beyond 40 mm/min negatively impairs the material flow (flow defect) and the weld's resultant strength. It is reckoned that at the highest traverse speed, the tool dwell or exposure time is short and this outcome is adjudged not to be suitable for sufficient inter-material flow and bonding. Paidar et al. [48] revealed that the improved flow/intermixing of material (material flow), and strong dislocation density were major factors responsible for the enhanced strength of the welded AA2024 alloy. Similarly, it has been reported that undesirable bonding and poor tensile strength are eliminated in the FSW'ed AA6061-T6/AA5754-O joint after achieving better material flow/intermixing and good metallurgical bonding [49]. The absence of root defects and the flow enhancement/consolidation of the SDFSW'ed joint are thus associated with its better performance over the single-sided friction stir welded counterparts.

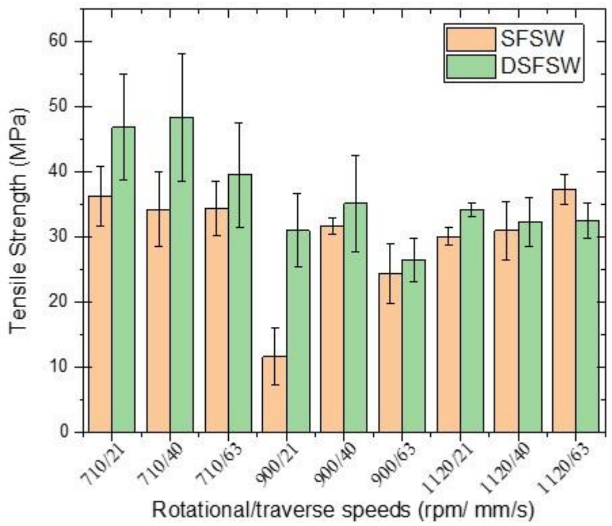

Figure 7. Tensile strength against the ratio of the rotating speed/travel or traverse speed in the SFSW and SDFSW-processed welds.

3.3 Fracture

Figure 8 shows the fracture locations and paths of the SFSW'ed and SDFSW'ed joints gotten at dissimilar welding parameters after the tensile loading process. The fracture location takes place at the stir zone of the SFSW'ed and SDFSW'ed joints regardless of the nature of the welds. This is because stress concentration is predominant at the weld zone of joints under uniaxial tensile loading circumstances. The uniformity of the tensile samples in terms of the inherent grain structure and height of the stirred zone is different from the unwelded part of the sample owing to the recrystallization, deformation, and shoulder-induced compression and shearing effects. This disparity at the stir zone is adjudged to have induced stress concentration at the centre of the SDFSW-processed welds during the loading process. Also, the occurrence of flow/root defects in the single-sided welds is adjudged to have localized the stress concentration and initiated cracking/failure at the stir zones. As a result, the observed fracture locations at the stir zones of the joints are justified. Meanwhile, stepped or zigzag fracture patterns are prominent in Figure 8 irrespective of the type of welds. The visual assessment of the fracture angle to the tensile direction was carried out. It was noted that a clear understanding of the fracture angle in relation to the process parameter is not discernible. This outcome might be due to the changes in the process parameter levels employed for joining the Al plates. To understand the fracture behaviour of the joints, the fractured samples were viewed in SEM.

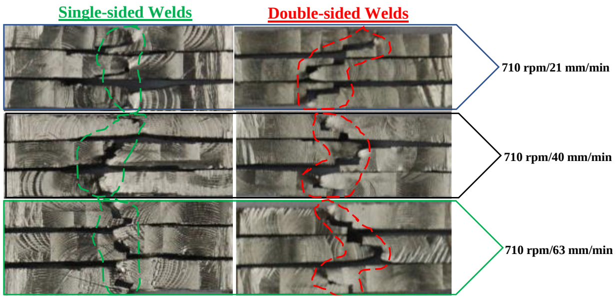

Figure 8. Fracture location and path of the SFSW'ed and SDFSW'ed joints.

However, it is pertinent to note that the defect zone is the favored spot for crack initiation in welds. The SEM images of the fractured SFSW and SDFSW'ed joints are consequently observed and presented in Figure 9. Brittle appearance with no obvious ductile features is dominant in the single-sided welds (see Figure 9a-d). A close assessment of Figure 9a-d shows that a characteristic transient breaking appearance or intergranular fracture is dominant in the SFSW'ed sample. This is an indication of a poor loadbearing attribute and this outcome is attributable to the inherent penetration-induced fractional unbonded margin or root defect in the SFSW'ed samples as compared to the SDFSW'ed sample. The elimination of the penetration-induced defect in the SDFSW'ed samples improves the loadbearing performance of the sample and leads to the observation of ductile features in the SEM images shown in Figure 9e-h. A higher number of dimples are present in Figure 9e-h compared to Figure 9a-d.

Stress concentration is expected at the penetration-induced fractional unbonded region (weld root) of the single-sided welds during the tensile assessment. The dominant stress at the fractional unbonded region of the weld is adjudged to have developed into a crack, leading to its eventual propagation through the stir zone of the welds. The growth of the crack into the stir zone is reckoned to have been responsible for the little or no dimples on the surfaces of the SFSW'ed welds revealed in Figure 9a-d. However, the SDFSW welds had some degrees of ductile features such as shallow dimples (see Figure 9e-h). It is consequently inferred that the elimination of the penetration-induced fractional unbonded region (root defect) in the SDFSW-processed welds is responsible for the ductile fracture appearance in the welds. The absence of such a defect caused a somewhat necking at the weld centre/stir zone of the joints during the axial tensile loading of the joints. Thus, the progressive increase in the tensile load led to necking-induced crack and eventual growth through the stir zone of the welds. Necking-induced failure was also described in the investigations of Heydari et al. [50]. This implies that some degree of loadbearing resistance is offered by the SDFSW'ed Al joints compared to the SFSW'ed Al joints. As a result, this justifies the presence of more shallow dimples and higher tensile strength in the SDFSW'ed joints relative to the SFSW'ed counterparts.

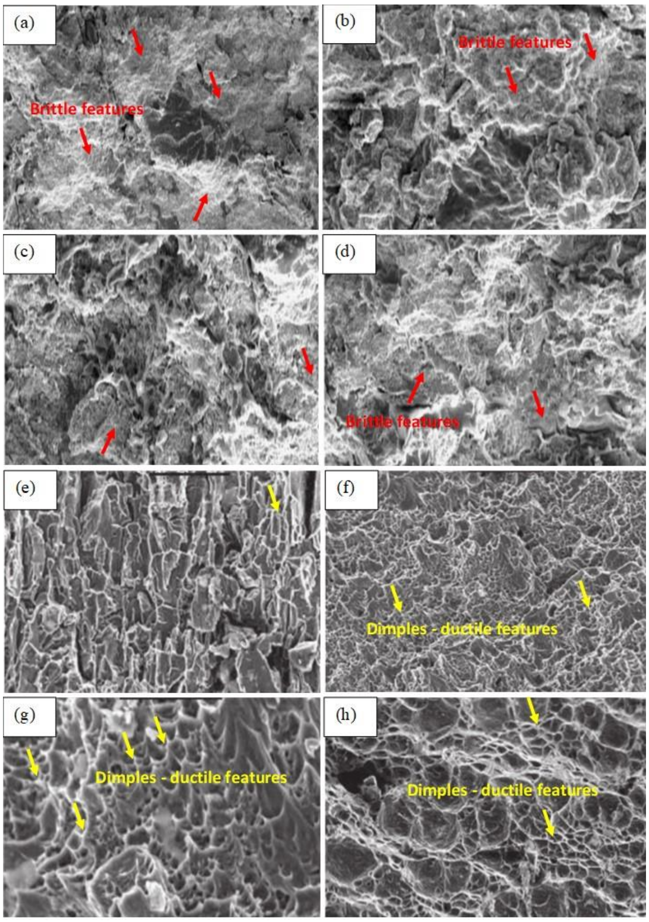

Figure 9. The fracture's SEM images of (a-d) single-sided welds, (e-h) double-sided welds.

4. Conclusion

The stepwise double-sided friction stir welded (SDFSW'ed) and single-sided friction stir welded (SFSW'ed) aluminium plates were compared in respect to microstructure, tensile strength, and fracture behaviours. The findings are summarized as follows:

i. The stepwise double-sided FSW process is a worthy approach to eliminating root defects in the solid-state joining of thick Al alloy.

ii. The stepwise double-sided FSW facilitates material flow consolidation and eliminates flow defects at the vortex region (pin tip) of the weld relative to the single-sided FSW process.

iii. Improved weld strength was obtained in the SDFSW'ed sample due to the two-sided deformation/material flow and elimination of penetration-induced fractional unbonded region or root defect.

iv. The highest tensile strength (48.41 MPa) was obtained at 710 rpm/40 mm/min after stepwise double-sided FSW of the Al alloy compared to the single-sided friction stir welded sample (34.24 MPa) due to defect elimination, and consolidated material flow with double-sided tool-assisted severe plastic-deformation and dynamic-crystallization effects.

v. A change of welding process from SDFSW to SFSW process does not meaningfully impact the fracture locations of the welded alloy owing to the weld zone acting as the stressed zone during the tensile test.

vi. Transient breaking (brittle) appearance and ductile fracture were observed in the single-sided FSW and stepwise double-sided FSW'ed Al samples respectively. These features correlate well with the tensile strength of the joints.

Author contributions

Olatunji Oladimeji Ojo: Conceptualization, Methodology, Reviewing and Editing. **Ozioma Alaba Oboro:** Data curation, Investigation, Writing-Original draft preparation.

Conflicts of interest

The authors declare no conflicts of interest.

References

1. Wang, Z. L., Zhang, Z., Xue, P., Ni, D. R., Ma, Z. Y., Hao, Y. F., Zhao, Y. H., & Wang, G. Q. (2022). Defect formation, microstructure evolution, and mechanical properties of bobbin tool friction–stir welded 2219-T8 alloy. *Materials Science and Engineering: A, 832*, 142414.
2. Bayazid, S. M., Farhangi, H., & Ghahramani, A. (2015). Effect of pin profile on defects of friction stir welded 7075 aluminium alloy. *Procedia Materials Science, 11*, 12–16.
3. Shirazi, H., Kheirandish, S., & Safarkhanian, M. A. (2015). Effect of process parameters on the macrostructure and defect formation in friction stir lap welding of AA5456 aluminium alloy. *Measurement, 76*, 62–69.
4. Ojo, O. O., Taban, E., Kaluc, E., & Sik, A. (2019). Cyclic lateral behavior of friction stir spot welds of AA2219 aluminium alloy: Impact of inherent flow defects. *Kovove Materialy, 57*, 329–342.
5. Ebrahimzadeh, V., Paidar, M., Safarkhanian, M. A., & Oladimeji, O. O. (2018). Orbital friction stir lap welding of AA5456-H321/AA5456-O aluminium alloys under varied parameters. *International Journal of Advanced Manufacturing Technology, 96*, 1237–1254.
6. Shankar, S., Saw, K., Chattopadhyaya, S., & Hloch, S. (2018). Investigation on different type of defects, temperature variation and mechanical properties of

friction stir welded lap joint of aluminium alloy 6101-T6. *Materials Today: Proceedings, 5*, 24378–24386.

7. Yi, T., Liu, S., Fang, C., & Jiang, G. (2020). Eliminating hole defects and improving microstructure and mechanical properties of friction stir welded joint of 2519 aluminium alloy via TIG arc. *Journal of Materials Processing Technology, 310*, 117773.
8. Wang, X., & Lados, D. A. (2022). Friction stir welding of similar aluminium alloys thick plates: Understanding the material flow, microstructure evolution, defect formation, and mechanical properties. *Materialia, 24*, 101508.
9. Mehrez, S., Paidar, M., Cooke, K., Vihnesh, R. V., & Ojo, O. O. (2021). Comparative study on weld characteristics of AA5083-H112 to AA6061-T6 sheets produced by MFSC and FSSW processes. *Vacuum, 190*, 110298.
10. Entringer, J., Meisnar, M., Reimann, M., Blawert, C., Zheludkevich, M., & dos Santos, J. F. (2019). The effect of grain boundary precipitates on stress corrosion cracking in a bobbin tool friction stir welded Al-Cu-Li alloy. *Materials Letters: X, 2*, 100014.
11. Xu, W., Wang, H., Luo, Y., Li, W., & Fu, M. W. (2018). Mechanical behavior of 7085-T7452 aluminium alloy thick plate joint produced by double-sided friction stir welding: Effect of welding parameters and strain rates. *Journal of Manufacturing Processes, 35*, 261–270.
12. Rahmatian, B., Dehghani, K., & Mirsalehi, S. E. (2020). Effect of adding SiC nanoparticles to nugget zone of thick AA5083 aluminium alloy joined by using double-sided friction stir welding. *Journal of Manufacturing Processes, 52*, 152–164.
13. Chen, J., Fujii, H., Sun, Y., Morisada, Y., & Ueji, R. (2013). Fine grained Mg–3Al–1Zn alloy with randomized texture in the double-sided friction stir welded joints. *Materials Science and Engineering: A, 580*, 83–91.
14. Khalid, E., Shunmugasamy, V. C., & Mansoor, B. (2022). Microstructure and tensile behavior of a bobbin friction stir welded magnesium alloy. *Materials Science and Engineering: A, 840*, 142861.
15. Shao, M., Wang, C., Zhang, H., Zhang, J., Liu, D., Wang, F., Ji, Y., & Chen, G. (2022). Microstructure and corrosion behavior of bobbin tool friction stir welded 2219 aluminium alloy. *Materials Characterization, 192*, 112178.
16. Fuse, K., & Badheka, V. (2021). Effect of shoulder diameter on bobbin tool friction stir welding of AA 6061-T6 alloy. *Materials Today: Proceedings, 42*, 810–815.
17. Wu, D., Li, W., Liu, X., Gao, Y., Wen, Q., & Vairis, A. (2021). Effect of material configuration and welding parameter on weld formability and mechanical properties of bobbin tool friction stir welded Al-Cu and Al-Mg aluminium alloys. *Materials Characterization, 182*, 111518.
18. Chu, Q., Li, W. Y., Wu, D., Liu, X. C., Hao, S. J., Zou, Y. F., Yang, X. W., & Vairis, A. (2021). In-depth understanding of material flow behavior and refinement mechanism during bobbin tool friction stir welding. *International Journal of Machine Tools and Manufacture, 171*, 103816.
19. Li, G. H., Zhou, L., Luo, S. F., Dong, F. B., & Guo, N. (2020). Quality improvement of bobbin tool friction stir welds in Mg-Zn-Zr alloy by adjusting tool geometry. *Journal of Materials Processing Technology, 282*, 116685.
20. Li, G. H., Zhou, L., Zhang, H. F., Guo, G. Z., Luo, S. F., & Guo, N. (2021). Evolution of grain structure, texture and mechanical properties of a Mg–Zn–Zr alloy in bobbin friction stir welding. *Materials Science and Engineering: A, 799*, 140267.
21. Sahu, P. K., Vasudevan, N. P., Das, B., & Pal, S. (2016). Assessment of self-reacting bobbin tool friction stir welding for joining AZ31 magnesium alloy at inert gas environment. *Journal of Magnesium and Alloys, 7*, 661–671.
22. Li, G., Zhou, L., Zhang, J., Luo, S., & Guo, N. (2014). Macrostructure, microstructure and mechanical properties of bobbin tool friction stir welded ZK60 Mg alloy joints. *Materials Research and Technology, 9*, 9348–9361.
23. Li, G., Zhou, L., Luo, S., Dong, F., & Guo, N. (2020). Microstructure and mechanical properties of bobbin tool friction stir welded ZK60 magnesium alloy. *Materials Science and Engineering: A, 776*, 138953.
24. Li, G., Zhou, L., Zhang, H., Luo, S., & Guo, N. (2021). Effects of traverse speed on weld formation, microstructure and mechanical properties of ZK60 Mg alloy joint by bobbin tool friction stir welding. *Chinese Journal of Aeronautics, 34*, 238–250.
25. Li, W. Y., Fu, T., Hütsch, L., Hilgert, J., Wang, F. F., dos Santos, J. F., & Huber, N. (2014). Effects of tool rotational and welding speed on microstructure and mechanical properties of bobbin-tool friction-stir welded Mg AZ31. *Materials & Design, 64*, 714–720.
26. Yang, C., Zhang, J. F., Ma, G. N., Wu, L. H., Zhang, X. M., He, G. Z., Xue, P., Ni, D. R., Xiao, B. L., Wang, K. S., & Ma, Z. Y. (2020). Microstructure and mechanical properties of double-side friction stir welded 6082Al ultra-thick plates. *Journal of Materials Science & Technology, 41*, 105–116.
27. Entringer, J., Reimann, M., Norman, A., & dos Santos, J. F. (2019). Influence of Cu/Li ratio on the microstructure evolution of bobbin-tool friction stir welded Al–Cu–Li alloys. *Journal of Materials Research and Technology, 8*, 2031–2040.
28. Chu, Q., Li, W. Y., Hou, H. L., Yang, X. W., Vairis, A., Wang, C., & Wang, W. B. (2019). On the double-side probeless friction stir spot welding of AA2198 Al-Li alloy. *Journal of Materials Science & Technology, 35*, 784–789.
29. Nosrati, H. G., Yazdani, N. M., & Khoran, M. (2022). Double-sided friction stir welding of AA 2024-T6 joints: Mathematical modeling and optimization. *CIRP Journal of Manufacturing Science and Technology, 36*, 1–11.
30. Azeez, S. T., & Akinlabi, E. T. (2018). Effect of processing parameters on microhardness and microstructure of a double-sided dissimilar friction stir welded AA6082-T6 and AA7075-T6 aluminium

alloy. *Materials Today: Proceedings, 5*, 18315–18324.

31. Ke, W. C., Oliveira, J. P., Ao, S. S., Teshome, F. B., Chen, L., Peng, B., & Zeng, Z. (2022). Thermal process and material flow during dissimilar double-sided friction stir spot welding of AZ31/ZK60 magnesium alloys. *Journal of Materials Research and Technology, 17*, 1942–1954.
32. Thakur, A., Sharma, V., & Bhadauria, S. S. (2021). Effect of tool tilt angle on weld joint strength and microstructural characterization of double-sided friction stir welding of AZ31B magnesium alloy. *CIRP Journal of Manufacturing Science and Technology, 35*, 132–145.
33. Darmadi, D. B., & Talice, M. (2011). Improving the strength of friction stir welded joint by double-side friction welding and varying pin geometry. *Engineering Science and Technology, an International Journal, 24*, 637–647.
34. Wang, F. F., Li, W. Y., Shen, J., Wen, Q., & dos Santos, J. F. (2018). Improving weld formability by a novel dual-rotation bobbin tool friction stir welding. *Journal of Materials Science & Technology, 34*, 135–139.
35. Chen, J., Ueji, R., & Fujii, H. (2015). Double-sided friction-stir welding of magnesium alloy with concave–convex tools for texture control. *Materials & Design, 76*, 181–189.
36. Wang, X., Morisada, Y., & Fujii, H. (2021). Interface strengthening in dissimilar double-sided friction stir spot welding of AZ31/ZK60 magnesium alloys by adjustable probes. *Journal of Materials Science & Technology, 85*, 158–168.
37. Wang, X., Morisada, Y., & Fujii, H. (2021). High-strength Fe/Al dissimilar joint with uniform nanometer-sized intermetallic compound layer and mechanical interlock formed by adjustable probes during double-sided friction stir spot welding. *Materials Science and Engineering: A, 809*, 141005.
38. Sun, Y., Fujii, H., & Morisada, Y. (2020). Double-sided friction stir welding of 40 mm thick low carbon steel plates using a pcBN rotating tool. *Journal of Manufacturing Processes, 50*, 319–328.
39. Yang, C., Ni, D. R., Xue, P., Xiao, B. L., Wang, W., Wang, K. S., & Ma, Z. Y. (2018). A comparative research on bobbin tool and conventional friction stir welding of Al-Mg-Si alloy plates. *Materials Characterization, 145*, 20–28.
40. Xu, W. F., & Liu, J. H. (2015). Microstructure evolution along thickness in double-side friction stir welded 7085 Al alloy. *Transactions of Nonferrous Metals Society of China, 25*, 3212–3222.
41. Wang, X., Morisada, Y., Ushioda, K., & Fujii, H. (2022). Double-sided friction stir spot welding of ultra-high strength C-Mn-Si martensitic steel by adjustable probes. *Journal of Materials Processing Technology, 300*, 117422.
42. Wang, X., Morisada, Y., & Fujii, H. (2021). Interface development and microstructure evolution during double-sided friction stir spot welding of magnesium alloy by adjustable probes and their effects on mechanical properties of the joint. *Journal of Materials Processing Technology, 294*, 117104.
43. Qiao, Q., Su, Y., Cao, H., Zhang, D., & Ouyang, Q. (2020). Effect of post-weld heat treatment on double-sided friction stir welded joint of 120 mm ultra-thick SiCp/Al composite plates. *Materials Characterization, 169*, 110668.
44. Ojo, O. O., Taban, E., & Kaluc, E. (2015). Friction stir spot welding of aluminium alloys: A recent review. *Materialpruefung/Materials Testing, 57*, 609–627.
45. Ojo, O. O., & Obasha, I. O. (2022). Modeling and optimization of friction stir stitching of AISI 201 stainless steel via Box-Behnken design methodology. *Production Engineering Archives, 28*, 132–140.
46. Ojo, O. O. (2019). Multi-objective optimization of friction stir spot welds of aluminium alloy using entropy measurement. *International Journal of Engineering Research in Africa, 45*, 28–41.
47. Oladimeji, O. O., Taban, E., & Kaluc, E. (2016). Understanding the role of welding parameters and tool profile on the morphology and properties of expelled flash of spot welds. *Materials & Design, 108*, 518–528.
48. Paidar, M., Kazemi, A., Mahrez, S., & Ojo, O. O. (2021). Investigation of modified friction stir clinching-brazing process of AA2024 Al/AZ31 Mg: Metallurgical and mechanical properties. *Archives of Civil and Mechanical Engineering, 21*, 115.
49. Paidar, M., Mehrez, S., Ojo, O. O., Mohanavel, V., Babaei, B., & Ravichandran, M. (2021). Modified friction stir clinching of AA6061-T6/AA5754-O joint: Effect of tool rotational speed and solution heat treatment on mechanical, microstructure, and fracture behaviors. *Materials Characterization, 173*, 110962.
50. Heydari, F., Amadeh, A. A., Ojo, O. O., Hasanniya, M. H., & Tamizifar, M. (2019). Microstructure and mechanical properties of autobody steel joined by friction stir spot welding. *Sadhana - Academy Proceedings in Engineering Sciences, 44*(3), 73.